In-situ rapid determination of walls' thermal conductivity, volumetric heat capacity, and thermal resistance, using response factors

Rasooli, A.; Itard, L.

DOI
10.1016/j.apenergy.2019.113539

Publication date
2019

Document Version
Final published version

Published in
Applied Energy

Applied Energy 253 (2019) 113539

Contents lists available at ScienceDirect

Applied Energy

journal homepage: www.elsevier.com/locate/apenergy

In-situ rapid determination of walls' thermal conductivity, volumetric heat capacity, and thermal resistance, using response factors

Arash Rasooli*, Laure Itard

OTB: Research for the Built Environment, Delft University of Technology, Julianalaan 134, 2628 BL Delft, the Netherlands

HIGHLIGHTS

- Rapid in-situ determination of thermal resistance via EPM is presented.
- Rapid in-situ determination of thermal conductivity and VHC of a wall is presented.
- Time interval should be selected based on the wall's minimum thermal response time.
- Properties of the different layers of a wall can be rapidly determined by EPM.

ARTICLE INFO

Keywords:
In-situ measurement
Thermal resistance
Excitation Pulse Method
Response factors
Transient heat transfer
Thermo-physical properties

ABSTRACT

Accurate determination of walls' thermo-physical characteristics is a necessity for execution of energy conservation strategies in existing buildings. In practice, such data is not available because the current determination methods are time expensive and therefore rarely used. Based on the theory of Response Factors, a rapid transient in-situ method, Excitation Pulse Method, EPM, was introduced as proof of concept in a former article. In the present article, detailed conditions for accurate application of the method in heavy and multi-layered walls are further studied. Theory, simulations, and experiments are combined to determine the method's performance in different types of walls, with specific attention to the effects of the walls' thermal response time and the response factors' time interval, leading to the accuracy of R_c-value determination. It is demonstrated that the two main thermo-physical properties of a wall, thermal conductivity and volumetric heat capacity, as well as the wall's thickness can be determined using inverse modelling of the Response Factors. The ratios of the response factors have shown to determine wall's minimum thermal response time and to give an indication of the wall's composition. The use of longer time intervals has shown to be advantageous in terms of the accuracy and the performance of the method. Longer experiment times as a result of long time intervals are still considerably shorter than the time required for making measurements according to the current standards and other conventional methods.

1. Introduction

Within the framework of the European Energy Performance of Building Directive (EPBD) [1], the lack of accurate input data regarding actual thermal performance of construction walls is considered as a bottle neck in the mandatory determination of buildings' energy performance. In addition to being the basis of policies and decisions regarding energy efficiency measures and energy saving targets [2], forecasting the buildings' energy performance is necessary for sizing of the HVAC facilities [3]. Along the same line, accurate estimation of the critical thermo-physical characteristics of buildings' façades as a result of the urge for energy audits [4] and energy performance checks is essential. To improve the thermal performance of the buildings, the building envelopes' thermal characteristics have been the first to be targeted [5]. The existing assumed values of these characteristics, such as walls' thermal resistance (R_c-value) have shown to be of the most critical parameters [6] contributing to the large deviations between actual and theoretical energy consumption [7]. Underestimation of the R_c-value has shown to result in around 400% overestimation in wall's thermal transmittance [8], leading to a high overestimation of the buildings' energy consumption [9]. Due to the absence of accurate and reliable data regarding actual thermo-physical characteristics, till today, the standard in-situ measurement methods [10–12] have been the most reliable option to follow. However, due to long measurement

* Corresponding author.
E-mail addresses: A.Rasooli@tudelft.nl (A. Rasooli), L.C.M.Itard@tudelft.nl (L. Itard).

https://doi.org/10.1016/j.apenergy.2019.113539
Received 23 April 2019; Received in revised form 14 June 2019; Accepted 11 July 2019

Nomenclature

Symbols

C	specific heat capacity ($J\,kg^{-1}\,K^{-1}$)
D	common ratio between two consecutive RFs
f	function of parameters
k	thermal conductivity ($W\,m^{-1}\,K^{-1}$)
L	wall thickness (m)
m	index where the RFs ratio become constant
n	maximum required number of RFs
$\dot{q}$	heat flux ($W\,m^{-2}$)
q	heat content ($J\,m^{-2}$)
R	electric resistance (Ω)
R_c	conductive thermal resistance ($m^2\,K\,W^{-1}$)
S	Surface area between a curve and the x-axis
T	temperature (K)
t	time (s) – time interval (half of the triangle's base)
U	multi-layered wall RF at excitation side ($W\,m^{-2}\,K^{-1}$)
V	multi-layered wall RF, opposite side of excitation ($W\,m^{-2}\,K^{-1}$)
Vo	voltage (V)
W	multi-layered wall RF at excitation side ($W\,m^{-2}\,K^{-1}$)
X	single layer RF at excitation side ($W\,m^{-2}\,K^{-1}$)
Y	single layer RF at the, opposite side of excitation ($W\,m^{-2}\,K^{-1}$)
Z	single layer RF at the exterior excitation side ($W\,m^{-2}\,K^{-1}$)

Greek letters

α	thermal diffusivity ($m^2\,s^{-1}$)
δ	magnitude of the triangular excitation signal (K)
λ	reduction factor for response time (%)
ρ	density ($kg\,m^{-3}$)
$\tau_r\|_{1-\lambda}$	thermal response time for $1-\lambda$ (s)

Indices

1, 2	layer number in a multi-layered wall
A	associated with indoor surface (excitation side)
B, C	associated with outdoor/middle surface (opposite side)
i	summation counter
j	RF index

Superscripts

$*$	obtained from the measurements

Abbreviations

DEP	Departure (%)
EPM	Excitation Pulse Method
RF	Response Factor
VHC = ρC	Volumetric Heat Capacity ($J\,m^{-3}\,K^{-1}$)

periods on the one hand and the many constraints of the test conditions on the other hand, the required time and effort are seldom feasible in practice and therefore, has become a barrier to their application. Consequently, efforts have been needed to assess the issue by developing and testing alternative measurement methods. Recently, the proof of principle of the Excitation Pulse Method (EPM) was presented, which allows for a relatively quick and accurate in-situ estimation of light walls' thermal resistance [8]. The objective of this article is to extend the method towards heavy walls and multi-layer walls, illustrate its accuracy and performance, and to demonstrate the capability of the method in the determination of other thermal properties: thermal conductivity and volumetric heat capacity (VHC). Additionally, the practical application of the theory of Response Factors (RFs) [13] is demonstrated.

1.1. State-of-the-art

Several approaches have been set up to estimate building components' thermo-physical characteristics. For walls of well-known construction, the R_c-value can be calculated following ISO 6946 [14]. However, as shown in numerous studies, the actual R_c-values often do not agree with the calculated ones [15] and the ones declared by the manufacturers. Therefore, much emphasis has been laid on performing measurements rather than calculations, to determine a more realistic thermal performance of the building components. For instance, in-lab measurement methods including the famous hot-box method by ISO 8990 [16] guarded hot plate apparatus by ASTM [17] have been applied in many cases [18–20]. Due to the often large variations between the in-situ and in-lab performance of the building components, as a result of in-situ conditions (e.g. moisture content and material aging), various in-situ effects including wind velocity [21], emissivity of the sensors, and large temperature drifts [22] have been included in the analysis of the test results, showing appreciable improvements.

As the most accurate approach in determination of buildings' actual thermo-physical characteristics, in-situ methods [8,11,12,23–26] have been given special attention as they measure and assess the realistic actual performance directly on site. Many pieces of research have been carried out during IEA Annex 58 (2011–2015) and IEA Annex 71 (2016–2021) regarding this topic as a result of its significance in the accurate indication of buildings' energy performance.

The non-contact measurement category of in-situ methods relates to IR thermography. This method has been applied by Fokaides and Kalogirou [27] to determine the thermal transmittance and later by Aversa et al. [28] to determine actual dynamic thermal behaviour of building components. Despite the advantage of being relatively simple to use, the quantitative application of this method is based on assumptions which may be far from actual circumstances. For instance, the emissivity of the surface as well as the air is required for an accurate estimation of the surface temperatures. Accordingly, Albatici et al. [29] improved this shortcoming by measuring and including the wind velocity and surface emissivity, showing how this method can be reliable in determination of thermal transmittance in heavy elements. More recently, Lucchi [30] reviewed 150 pieces of literature about this technique, suggesting relevant procedures and tool development for dynamic characterization of building components.

Direct contact, being widely applied, the most important in-situ wall characterization method is the standard heat flow meter method introduced in ISO 9869 [10] and ASTM [11,12]. The method has been of preference as the international reference and it benefits from a quite straight-forward procedure. However, this method has often shown to rely on very long (up to more than a month) measurement periods [4,25,31–34]. Moreover, low temperature gradients between the two sides of the walls have shown a significantly negative effect on the accuracy of the method. In line with the results of Desogus et al. [35], Atsonios et al. [23] have shown that the method is not reliable in low temperature gradients. Accordingly, many studies have suggested and developed corrections by means of practical extensions [25] and dynamic data analysis methods to shorten the measurement periods and to overcome the accuracy drawback. Using dynamic data analysis and alternative interpretation methods [26], it has been possible to successfully calculate the thermal resistance [36] and thermal transmittance [37] in shorter periods of time.

Including materials' detailed thermal properties (which are often not required for the long measurements periods) to study the dynamic behaviour [38] of buildings has resulted in significant improvements [39]. Lately, Petojević et al. [40] introduced a new mathematical framework by which the dynamic thermal characteristics of multi-layered walls (excluding cavity walls) can be determined, using days of heat flux and temperature measurements. In contrast with general findings in literature, Evangelisti et al. [41] found an acceptable agreement between the dynamic thermal behaviour of a homogeneous wall, which was modelled as an equivalent to a multi-layered one of the same thermal performance. Applying finite difference method and experimental data of 50 h, the properties were found to be representative for the wall of unknown construction. Most recently, Šuklje et al. [42] calibrated a homogeneous equivalent wall model for inverse determination of thermo-physical properties in green facades. Along the same line, the use of other dynamic-theory-based methods such as signal-response methods has been suggested. The idea of using excitation of a system and studying its response is being used widely in the level of the whole buildings [43]. The main methods associated with this technique include the QUB [44] and ISABELE [45] which estimate the global heat lost coefficient of a whole building [46]. Similarly, for the scale of building components (e.g. walls) the RF method has been considered. The RF method, first developed by Mitalas and Stephenson [13] has shown to be a suitable alternative to solving heat equations. The method is solely based on a temperature excitation on a system and its corresponding heat flux response and in many situations is less expensive than the numerical methods, in terms of computation time [47]. Many studies have proposed alternative mathematical methods such as direct numerical integration [48] and state space method [49] for calculation of RFs in multi-layered walls [50] even more efficiently. Apart from walls' heat transfer analysis, the applications of the RF method ranges from the assessment of the thermal performance of capillary radiant floors [51] and earth-to-air heat exchangers [52] to thermal behaviour of food products [53]. The RF method has been experimentally applied in lab conditions on walls in 2008 via a calibrated hot-box by Sala et al. [54] to test a multi-layered heterogeneous wall. The study showed the significant difference in results when the heterogeneous layer of hollow brick is modelled as a homogeneous layer, equivalent to the heterogeneous one. Later in 2010, Martin et al. [55] used the same apparatus to measure and calculate the RFs of walls of low thermal resistance and medium thermal inertia. The R_c-value has been measured once through steady-state regime and once via the RFs through a dynamic regime. The method was compared to the computational model, showing a good agreement. The authors found the method to be a suitable alternative when the properties of the tested wall are unknown.

In-situ determination of thermo-physical properties has so far taken days of in-situ measurements. In the current article, a transient in-situ method is demonstrated, by which, at least in many cases (light to medium weighted walls), it is possible to determine the thermal resistance R_c-value, thermal conductivity, Volumetric Heat Capacity, and an indication of possible construction of an unknown wall, within a few hours, without the many constraints required by the conventional methods.

1.2. Excitation Pulse Method, EPM

Aiming for rapid determination of the walls' thermal resistance R_c-value, a rapid transient-based in-situ measurement method, EPM, based on the theory of RFs, was developed and tested on three case studies [8,56]. Applying the EPM, it was shown that by exposing one surface of a wall to a triangular temperature pulse under certain conditions, it is possible to estimate its thermal resistance in a few hours. In the theory of RFs, the excitation pulse is defined as a unit (1 K) magnitude (triangle's height) and the RFs time interval (half of the triangle's base) is typically one hour. The theory of RFs is based on Laplace transform, and thanks to superposition principle, the theory itself and therefore the EPM benefit similarly from temperature pulses of larger magnitudes. In EPM, the magnitude of the triangular excitation pulse (δ) is way above 1 K, in order to overcome the effect of walls' surface temperature and heat flux noise. The pulse magnitude δ is the difference between the initial value and the peak of the surface temperature at the excitation side.

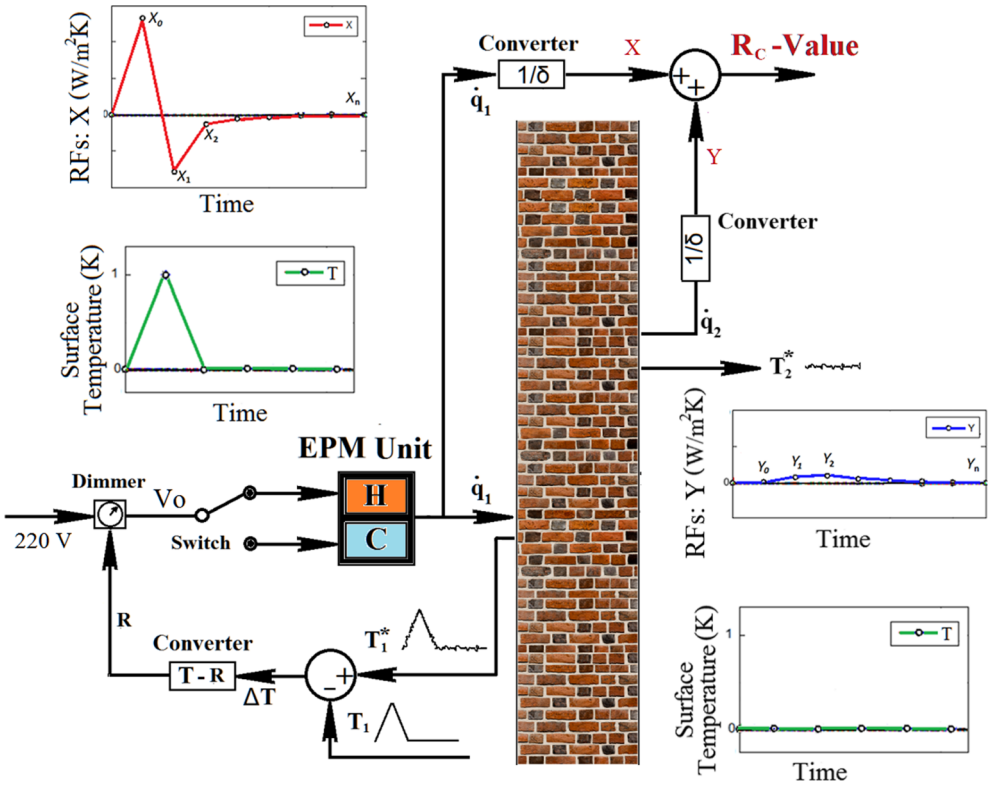

Fig. 1. Control system and working principles of EPM: The heat fluxes are controlled (and measured) in such a way that a triangular temperature excitation pulse forms on one side of the wall, while the other side is kept at constant temperature. The RFs are then calculated to be used for estimation of the wall's thermo-physical characteristic.

Working principles and the control circuit

The working principle of EPM is depicted in Fig. 1. Either manually or automatically, the control of the heating and cooling units is performed to achieve a pre-defined triangular surface temperature profile T_1 as an excitation pulse on the wall. Here, the initial and the final wall's surface temperature are the equivalent of 0 K in the theory. A dimmer constrains and controls the voltage *Vo* towards the EPM unit to control the power for heating and cooling heat flux $\dot{q}_1$ in such a way that a measured triangular surface temperature T_1^*, following a desired triangular surface temperature profile T_1 with a height of δ is formed on the excited side (1) of the wall. A peak indoor surface temperature of 80–90 °C is generally found suitable for a safe experiment, not damaging the walls' finishing. Right after the peak, the surface heat flux $\dot{q}_1$ is decreased in such a way that the surface temperature profile declines linearly with an opposite slope. At the end of heat exertion ($\dot{q}_1$=0), the surface temperature is still above the base of the triangle (initial value), due to the effect of thermal storage. Therefore, at this point, to return to the initial temperature, heat removal takes place after switching the power from the heater to the cooler. The cooling is similarly controlled in such a way that the surface temperature reaches the base of the triangle, following the previous slope. At the end of the triangle, the temperature is kept at base to resemble the pulse at a zero level. At the opposite side of the wall, a protective box (60 × 60 cm^2, polystyrene covered with bubble wrap and reflective coating) is mounted to cover and protect a large area of the wall from the outdoor heat flux and temperature disturbances. Despite the success in reaching the purpose with the current size, the area of the box may be as large as possible. This way, the outdoor surface temperature T_2^* can remain at a constant level and the outdoor heat flux response $\dot{q}_2$ can be observed and measured, similar to the theory of RFs. Due to the outdoor conditions and the small size of outdoor heat flux, the results of outdoor heat flux are seldom analysed for extraction of wall's properties.

The whole control process takes place at very short time steps by comparing and minimizing the difference between the measured triangular surface temperature profile T_1^* and the pre-defined triangular temperature profile T_1. T_1^* is controlled via the converter that tunes the electrical resistance R of the dimmer. In the meantime, the surface heat fluxes at the excitation side ($\dot{q}_1$) and at the opposite side ($\dot{q}_2$) are measured via sets of heat flux meters mounted on the surface of the wall. All controls and conversions can take place manually or by using electronic systems. To obtain the wall's RFs, at every time interval, the heat fluxes are divided by the magnitude of the pulse δ, whose value is obtained from the thermocouple mounted on the excitation side of the wall

$$X_j = \frac{(\dot{q}_1)_j}{\delta};\ Y_j = \frac{(\dot{q}_2)_j}{\delta} \tag{1}$$

where X and Y are the RFs of the wall and j is the index indicating the time interval at which the heat flux must be used in terms of number of RFs (See Fig. 1). The R_c-value can be then obtained, using RFs of one side of the wall:

$$R_c = 1/\sum_{j=0}^{n} X_j = 1/\sum_{j=0}^{n} Y_j \tag{2}$$

or more quickly, when possible, using the RFs from both sides [8]:

$$R_c = 2 \times \left(\sum_{j=0}^{n} (X_j + Y_j)\right)^{-1} \tag{3}$$

In the current study, emphasis is laid solely on using X RFs for a variety of reasons. The Y RFs appear after the minimum response time (See Section 3.1), making the experiment longer, resulting in less feasibility. In addition, in heavy constructions and high insulation values, Y RFs are unlikely to be observed. The operational and instrumental errors associated with X RFs are much lower since the interior side of the wall is generally exposed to fewer sources of heat flux disturbance and therefore is better controlled. Nevertheless, the Y factors can be used for light walls in stable climatic conditions or in labs where the conditions on the outdoor wall can be fully controlled.

Location of the pulse and the size of the heated area

So far, EPM has been successfully applied to light homogeneous walls [8]. The results of simulations and experiments carried out so far have shown negligible difference between theory, computations, and experiments, in terms of walls' thermal behaviour and determination of the thermal resistance. The location of the pulse has to be as far as possible from the areas potentially disturbing the 1D signal and its response by 3D heat sink effects (e.g. wall area close to a window). An IR thermography camera should be used to check the homogeneity of heat flux (an indication for homogeneous surface temperature). The size of the heated area needs to be as large as possible. The heat fluxes and the temperatures should be measured then in the centre of this area, where the occurrence of heat transfer towards lateral sides is minimum. In case of presence of high insulation, the risk of 3D heat transfer increases. This can also be dealt with, heating an as large as possible surface. Practical details regarding the built prototype, properties of the triangular pulse, and the size of the heated area in relation with their effect on the accuracy of the method are discussed in [57]. It has also been shown how the accuracy of the method in finding the R_c-value increases when larger numbers of RFs or longer time intervals are used.

Although EPM has been demonstrated on 3 samples (walls of relatively light construction) [8], further research has been required to examine the method in more detail regarding its overall reliability and performance in other typologies as well as its further new applications. In the current article, the remaining main questions are addressed:

1. With regards to the thermal response time, applying which combinations of signal magnitude and time interval can lead to an accurate determination of the thermal resistance?
2. To what extend can the RFs of a wall help to understand and illustrate its construction and thermal behaviour?
3. To what extent is it possible in EPM to concurrently measure thermo-physical properties other than the R_c-value?

At first, the effect of a wall's response time and the selected signal time interval on the wall's RFs in single-layered and multi-layered walls is studied and specific RF features are illustrated, focusing on clarification of experimental and practical aspects and the potential future benefits of EPM and other RF- measurement methods. Secondly, aiming for more reliable estimations of thermal properties, the method is extended from the determination of the R_c-value to in-situ determination of two main fundamental thermo-physical properties: thermal conductivity and VHC. Unlike the R_c-value which is used in steady-state assumptions, these two properties are used in combination in dynamic modelling [38] of building components. It is shown to what extent the method at its current stage (manual control and basic equipment) can be used to determine the aforementioned material properties (as well as the wall thickness) for a tested wall.

2. Methodology

A combination of software simulations and experiments is used to answer the research questions and to explore boundaries, validity domain, and further application range of the method.

2.1. Simulations and computations

To avoid too long experiments, a large part of the study has been conducted using virtual walls and a virtual triangular pulse excitation,

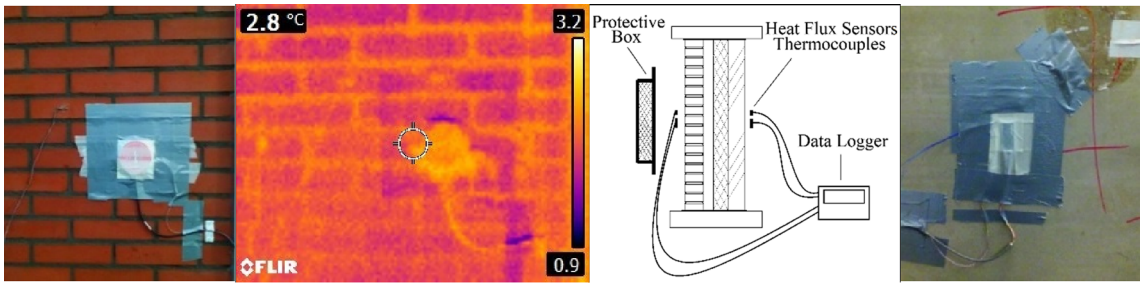

Fig. 2. From left to right: outdoor sensors and their IR image (under the protective box), the schematic of the equipment and the wall, indoor sensors, Dec 2018, Leuven, Belgium.

all modelled using COMSOL Multiphysics 5.3a [58]. The models have been computationally tested and validated using different approaches:

1- A single layer wall is modelled in COMSOL Multiphysics 5.3a: A wall of which one surface is exposed to a triangular temperature pulse of 1 K height, while its other side is kept at 0 K, is modelled. The heat fluxes at two sides are computed, representing the RFs.
2- These RFs are compared to the RFs from the theory [13] (calculated in MATLAB) as a function of wall's thermal properties and same time interval, showing excellent agreement.
3- The models for multi-layered walls were first validated by using identical layers and comparing them with an equivalent homogeneous wall of same material which is already validated in 1 and 2.
4- The magnitude of the signal is increased and using the realistic boundary conditions, the results are compared to the original model with 1 K magnitude, confirming the superposition rule with perfect agreement.

Other boundary conditions include lateral insulation. The initial condition of all solid domains is 0 K.

To maintain high accuracy, the "finer" mesh setting has been used for all simulations. The time stepping is chosen according to the mesh size. In multi-layered walls, the effect of thermal contact between layers has been tested beforehand. Due to the size of the constructions, for this method, imperfect thermal contact has shown no difference with perfect contact and therefore has been used in order to shorten the computation time.

2.2. Experiments

For the experiments, two heat flux sensors (HukseFlux HFP01 [59] for outdoor surface and EKO MF-180 [60] for indoor surface) and two high-accuracy (0.5 °C) T-type thermocouples, all pre-calibrated, have been used. The reason for using two different heat flux sensors is that the one for outside surface captures very small noise and the other for inside can handle high operational temperature. The two heat flux sensors have been calibrated and tested beforehand and had assured to give identical results. During the experiments, each thermocouple has been installed next a heat flux sensor, on both sides of the wall (Following the sensor installation guidelines of ISO 9869 [10]). Data have been logged using an OMEGA OM-SQ2010 high accuracy data logger. Before execution, IR thermography has been carried out using a FLIR E5 [61] IR camera to inspect and avoid possible discrepancies in surface temperature and heat flux. This check is necessary also after covering the sensors with a cover of same thermal emissivity as the wall's surface, to assure the same radiative heat transfer on the sensor and the surrounding surface. In Fig. 2, from left to right, the outdoor sensors (under the protective box), the IR image of the outdoor sensor, the schematic of the wall (Table 1) and the measurement equipment, and the indoor sensors are shown.

Measurements have been carried out using a prototype on a wall in a test-building laboratory in KU Leuven, Belgium. The following tests have been carried out to further study and validate the method:

- Comparison between the in-situ measured heat flux and the one computed in a theoretical model
- Comparison between measured X-RFs and time intervals for four different pulses
- Comparison between the results of two similar tests (precision)
- Comparison between the experimentally determined values for k and ρC in different pulses (precision)
- Comparison between the theoretical values k and ρC and the ones experimentally determined (accuracy)

In Table 1, the construction of the tested wall (from outside to inside) are tabulated in detail as presented in [62]. ρ is density, C is specific heat capacity, k is thermal conductivity, L is thickness, and $\tau_r|_{1\%}$ is the minimum response time (See Section 3.2). The results of the tests are shown in Fig. 5 and are used in the analyses carried out in Sections 3 and 4:

2.3. Experimental validation of the models

To validate the experimental models, the tested cavity wall (Table 1) has been modelled in COMSOL Multiphysics 3a [58]. The lateral sides are insulated and the entire surface is excited with a temperature pulse. The model is fed with the experimental temperature pulse data (Fig. 3, left), taken from the in-situ measurements from Test 4. The heat flux is then computed at the location of the heat flux sensors and compared to the ones measured on site (Fig. 3, right).

As seen from the agreement of the two heat flux profiles, the simulation model is in good agreement with the experiment. The differences between the profiles can be minimized by decreasing the mesh size, at the expense of long computational time.

In Section 3, the influence of the thermal response time on the required signal's time interval and its corresponding RFs is studied for

Table 1
Thermal properties of the tested wall.

Layer/property	L [m]	k [W m^{-1} K^{-1}]	ρ [kg m^{-3}]	C [J kg^{-1} K^{-1}]	$\tau_r\|_{1\%}$ [min]
Facing brick	0.10	0.900	2087	870	34.3
Air cavity	0.04	–	–	–	–
Polyurethane	0.10	0.021	35	1320	37.5
Wood-cement board	0.09	0.350	1250	1470	72.5

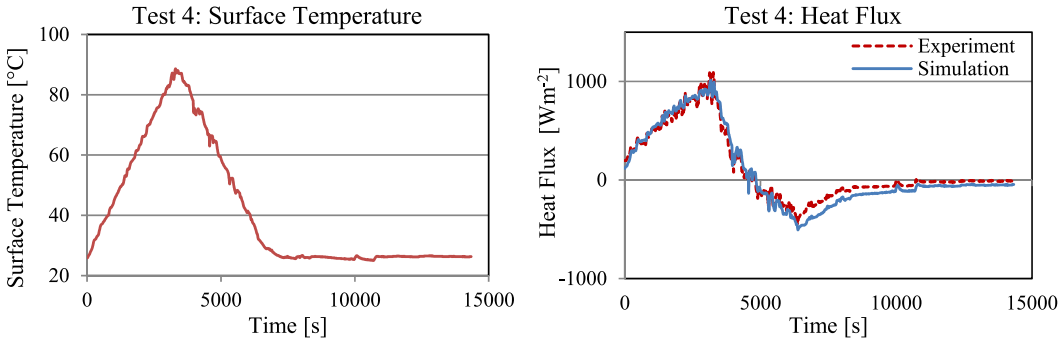

Fig. 3. Comparison between heat flux profiles (right) from the measurement (dashed red) and simulation (solid blue) from the surface temperature excitation pulse (left) being applied in the experiment and fed to the COMSOL model.

single-layered and double-layered constructions. Experiments show the possibility of carrying out measurements using triangular pulses of different time intervals and magnitudes. In addition to the determination of the minimum thermal response time, the ratios of the X RFs have shown to give an indication of presence of different layers in a multi-layered wall.

In Section 4, the results of the experiments have been used in an inverse modelling problem to determine the two main thermo-physical properties of a wall: thermal conductivity and VHC, as well as the thickness of a homogeneous slab.

3. RF time interval and the walls' thermal response time

3.1. EPM: RF time interval and pulse magnitude

To limit the required measurement time, the choice of the signal's time interval is critical for EPM. An appropriate time interval should be chosen before starting the measurements. The sufficiency of heat penetration through the wall depends on two aspects of time and heat flux. Accordingly, in practice, to ensure sufficient heat penetration (to observe the Y factors), to minimize the 3D heat transfer effects, and to overcome the surface heat flux noise, two different approaches can be followed: By exerting the excitation pulse on a large area, with a large magnitude δ (grey curves) and/or by choosing a long time interval. The quantity of heat q transferred to the wall during the pulse is equal to the area under the curve of heat flux-time.

$$q = \int_0^t \dot{q}(t)dt = \int_0^t \delta.\, X(t)dt \tag{4}$$

As shown in Fig. 4, for a light wall, by selecting a longer time interval (in light blue), in comparison to a shorter one (in orange) of the same pulse magnitude, a larger quantity of heat can be transferred to the wall. This has the same effect as imposing a larger magnitude with the short time interval (in dark red), resulting in a greater heat flux:

$$q = \int_A^C \dot{q}_{AB'C}(t)dt = S_{AB'C} = \int_A^E \dot{q}_{ADE}(t)dt = S_{ADE} \tag{5}$$

For a medium-weighted wall, a larger time interval in combination with a large pulse magnitude (dark blue) can support sufficient heat penetration through the body of the element.

$$\int_A^E \dot{q}_{AD'E}(t)dt > \int_A^C \dot{q}_{AB'C}(t)dt > \int_A^C \dot{q}_{ABC}(t)dt \tag{6}$$

Finally, for heavy constructions, longest possible time intervals

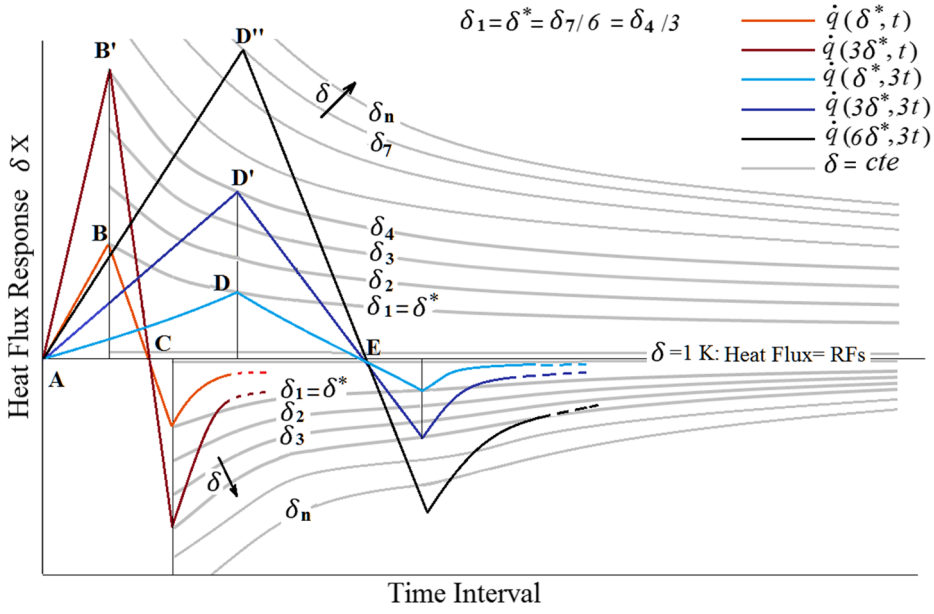

Fig. 4. Representation of excitation pulse magnitudes, time intervals and heat flux responses.

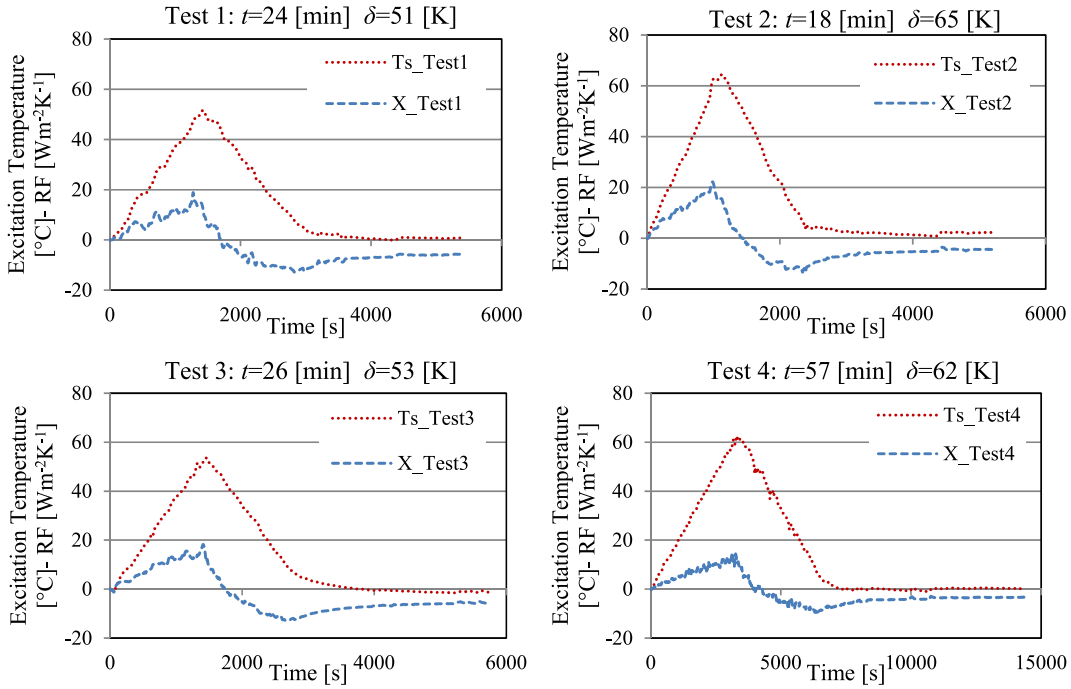

Fig. 5. Surface temperature (dotted red) and RFs (dashed blue) measurements in four experiments used in the analyses.

(longer than 1 h) and largest pulse magnitudes (90–100 °C) are to be used (in black).

$$\int_{A}^{E} \dot{q}_{AD''E}(t)dt \gg \int_{A}^{C} \dot{q}_{ABC}(t)dt \tag{7}$$

Applying such a large excitation pulse on a large area can increase the chance of observation of Y RFs, minimizing the risk of 3D heat transfer effects on 1D heat transfer of the pulse.

The constant δ grey lines represent the variations of X_0 and X_1 when t is increased.

In Fig. 5, the results of the measurements are presented. The red dotted curves are surface temperature pulse (above the initial and final surface temperature) at the excitation side and the dashed blue curves are the corresponding RFs (derived from the heat flux measurements and the pulse magnitude). It is shown how different combinations of δ the pulse magnitude and t the time interval can be applied in EPM. Note that tests 1 and 3 are very similar in terms of the two aforementioned parameters. In Section 4 it is shown how these two tests lead to the same results. Tests 2 and 4 are the shortest and longest experiments respectively.

By choosing a longer time interval, lower amplitude of heat flux is needed to take the surface temperature to 1 K. Accordingly, the RFs become naturally smaller. In Fig. 6, a concrete wall, exposed to an excitation pulse of 1 K is simulated. As seen from the curves, the X factors decrease as the time interval of the signal increases.

Similarly, the relation between the time interval and the magnitude of the excitation pulse and the corresponding RFs has been studied in the experiments. The experimental results of the RFs are shown in Fig. 7, where the black dashed and dotted-dashed lines present the X_0 and X_1 values. The X RFs become smaller as a larger time interval is applied.

Using a larger time interval has shown to be advantageous as in practice, as it leads to easier control of the triangular temperature profile. Since in this case the RFs are smaller, it is important to combine a longer time interval with large pulse magnitudes to ensure the distinction between the heat flux and temperature noise and the pulse and its response.

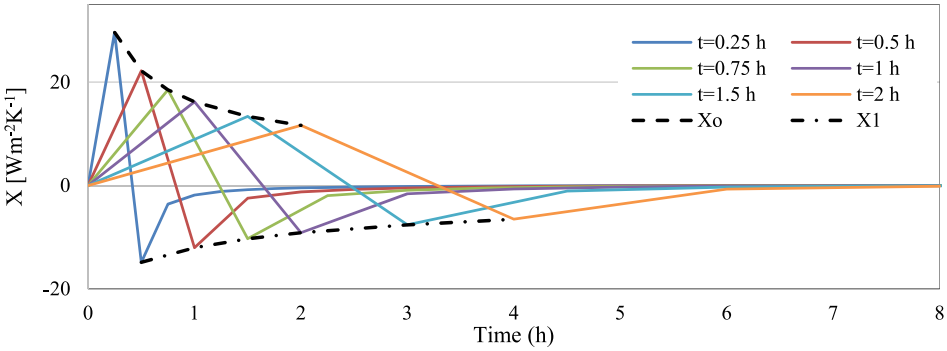

Fig. 6. Relation between different time intervals and RFs (X_0 in black dotted and X_1 in black dotted-dashed), data obtained from MATLAB computation of RF equations.

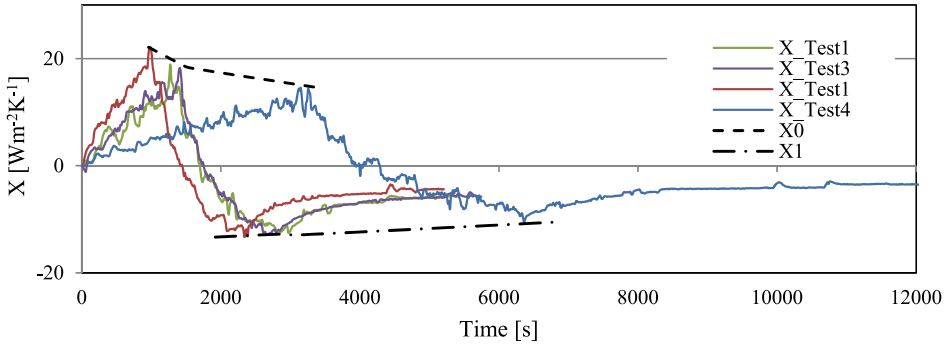

Fig. 7. Relation between different time intervals and RFs (X_0 in black dotted and X_1 in black dotted-dashed), data obtained from the experiments, Dec 2018, Leuven, Belgium.

3.2. Wall's thermal response time

The correct understanding of a wall's thermal behaviour, when submitted to a triangular excitation pulse, is achieved by the analysis of the thermal response time. The response time of a system is defined as the time required for the output to reach a certain percentage of the input, when the input is increased with a step function. For a homogeneous wall, considering the input as heat flux at excitation side, and the output being the heat flux at the other side, the thermal response time can be obtained by solving Fourier's heat equation. Accordingly, the response time of such wall of thickness L and thermal diffusivity α can be obtained as follows [63]:

$$\tau_r|_{1-\lambda} = \frac{4L^2}{\alpha\pi^2}\ln\frac{4}{\lambda\pi} \tag{8}$$

λ is the reduction factor to determine for output heat flux $\dot{q}_2$ to reach $(1-\lambda)\dot{q}_1$ during its response time $\tau_r|_{1-\lambda}$, when $\dot{q}_1$ is increased by one step. In Fig. 8, the response times of a brick wall ($k = 0.9$ W^{-1} K^{-1}, VHC = 1.36 E7) of different thicknesses L are shown. At $\lambda = 0.37$ the response time $\tau_r|_{63\%}$ is called "time constant", a well-known concept used when analogizing the thermal systems with electrical systems.

During a measurement using EPM and any other pulse-response-based method, it is highly important that the effect of the excitation side heat pulse reaches the other side. The minimum response time $\tau_r|_{1\%}$ (the required time for output heat flux-at the other side- to reach at least 1% of the input heat flux) happening at $\lambda = 0.99$ is critical to be covered by the time interval during the experiment. The minimum thermal response time $\tau_r|_{1\%}$ in a wall exposed to EPM is equal to the time required for the Y curve to rise from zero to positive values. This can be found during an experiment, provided that an adequate amount of heat is transferred to the surface of the wall (See Section 3.1). In many cases it is of necessity or at least beneficial to choose the time interval based on minimum thermal response time in order to avoid repetition of the experiment. The minimum response time can always be observed from the rise of the Y RF curve. Alternatively, it can be simply measured in a test in advance, by applying any form of excitation heat pulse at one side and log the time duration taking the other side of the wall to show a heat flux response. Furthermore, the minimum response time can be found by studying the ratio of the X RFs of high indices (See Section 3.5).

3.3. Response time and RFs' time interval: single-layered homogeneous walls

The effect of the excitation temperature pulse being applied to the first side of a wall needs at least a period of $\tau_r|_{1\%}$ to reach the second surface. When the second surface is reached, its heat flux increases (Y appears), acting as a heat flux pulse on this side. Similarly, this signal needs a period of $\tau_r|_{1\%}$ to reach back to the excitation side. If the time duration of the excitation signal is shorter than $2\tau_r|_{1\%}$, the effect of the second surface may not be transferred back to the results of heat flux response at the excitation side. For instance, consider a case where a time interval (time needed for appearance of X_0, the first RF) shorter than $2\tau_r|_{1\%}$ is used. At the time when X_0 is reached, the heat pulse effect is in the same location inside the wall, regardless of its thickness. Consequently, using such time interval will lead to identical X_0 values for the considered wall and a similar wall of much higher thickness. This implies that for very thick walls or the ones of high thermal mass (long response time), unless a very long time interval is used, X_0 does not depend on and therefore do not represent the thickness. In Table 2, the X_0 factors have been computed for different thicknesses and time intervals corresponding to the following conditions:

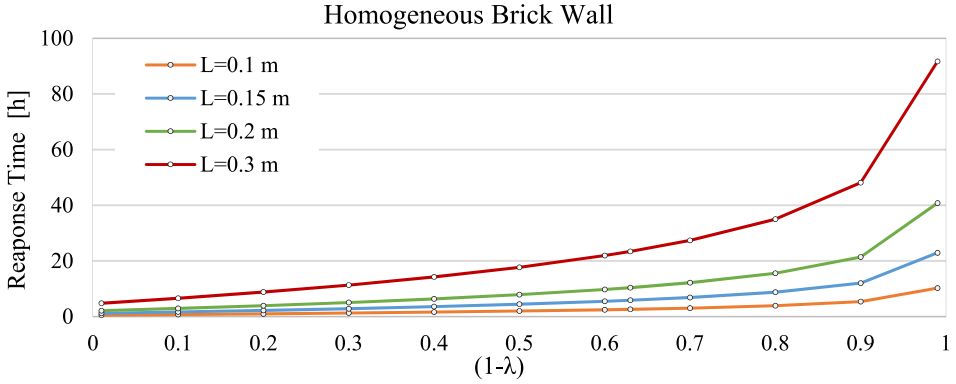

Fig. 8. Computation results: thermal response times of a homogeneous brick wall in different thicknesses (time constant is found at $(1-\lambda) = 0.63$).

Table 2
X_0 computed with the simulation model, for a brick wall ($k = 0.9$ W^{-1} K^{-1}, VHC = 136 E5) of different thicknesses (and different response times) using different time intervals.

	RF time interval [s]	$t = 10$	$t = 600$	$t = 1800$	$t = 3600$	$t = 180000$
Wall Thickness [m]	$\tau_r\|_{1\%}$[s]	$X_0\|_{t=10s}$	$X_0\|_{t=600s}$	$X_0\|_{t=1800s}$	$X_0\|_{t=3600s}$	$X_0\|_{t=180000s}$
0.01	18	**438.0**	99,3	93.1	91.5	90.0
0.05	457	**438.0**	**56.6**	33.3	25.7	18.0
0.1	1827	**438.0**	**56.6**	**32.7**	**23.1**	9.3
0.2	7310	**438.0**	**56.6**	**32.7**	**23.1**	5.1
0.5	45,687	**438.0**	**56.6**	**32.7**	**23.1**	**3.3**
0.8	116,961	**438.0**	**56.6**	**32.7**	**23.1**	**3.2**
1 >	> 182,751	**438.0**	**56.6**	**32.7**	**23.1**	**3.2**

The X_0 values in bold signify the identical values in the same time interval.

$$\begin{aligned} &t < \tau_r|_{1\%}: \begin{cases} X_0 \neq f(L) \\ Y_o = 0 \end{cases}; \\ &t < 2\tau_r|_{1\%}: \begin{cases} X_0 \neq f(L) \\ Y_o \geq 0 \end{cases}; \\ &t \geq 2\tau_r|_{1\%}: \begin{cases} X_0 = f(L) \\ Y_o > 0 \end{cases} \end{aligned} \tag{9}$$

As seen in Table 2, as long as the selected time interval is shorter than $2\tau_r|_{1\%}$, the X_0 in walls of different thicknesses will be identical. Note that in all given conditions (except for $t = 10$ s which is extremely short), it may still be possible to successfully extract the R_c-value from the RFs, provided that at some point in the rest of the RFs with higher index, $2\tau_r|_{1\%}$ has been passed in time, changing the rest of the RFs. This, in heavy walls may demand for a very long experiment time. Similarly, the aforementioned interpretation is valid for the RFs of higher index: If $2\tau_r|_{1\%}$ is not reached during the appearance of any X RF (of higher index), that X RF and the ones before (smaller indices) are also identical for walls of any higher thickness:

$$\begin{aligned} &(j+1)t < 2\tau_r|_{1\%}: \begin{cases} X_j \neq f(L) \\ Y_o \geq 0 \end{cases}; \\ &(j+1)t \geq 2\tau_r|_{1\%}: \begin{cases} X_j = f(L) \\ Y_o > 0 \end{cases} \end{aligned} \tag{10}$$

$$\begin{cases} q_A^t = [T_A^t \cdots T_A^{t-n}] \begin{bmatrix} X_0 \\ \vdots \\ X_n \end{bmatrix}_{(1)} - [T_B^t \cdots T_B^{t-n}] \begin{bmatrix} Y_0 \\ \vdots \\ Y_n \end{bmatrix}_{(1)} \\ q_B^t = [T_A^t \cdots T_A^{t-n}] \begin{bmatrix} Y_0 \\ \vdots \\ Y_n \end{bmatrix}_{(1)} - [T_B^t \cdots T_B^{t-n}] \begin{bmatrix} X_0 \\ \vdots \\ X_n \end{bmatrix}_{(1)} = q_B^t = [T_B^t \cdots T_B^{t-n}] \begin{bmatrix} X_0 \\ \vdots \\ X_n \end{bmatrix}_{(2)} - [T_c^t \cdots T_c^{t-n}] \begin{bmatrix} Y_0 \\ \vdots \\ Y_n \end{bmatrix}_{(2)} \\ q_C^t = [T_B^t \cdots T_B^{t-n}] \begin{bmatrix} Y_0 \\ \vdots \\ Y_n \end{bmatrix}_{(2)} - [T_C^t \cdots T_C^{t-n}] \begin{bmatrix} X_0 \\ \vdots \\ X_n \end{bmatrix}_{(2)} \end{cases} \tag{11}$$

This implies that when using a short time interval and measuring a limited number of RFs, the RF curves of walls of different thicknesses can be identical and therefore, the accuracy of R_c-value determination can become extremely poor as the RFs do not include enough information about the thickness of the tested wall.

Note that in theory, unlike in practice, numerous RFs can be used. Accordingly, the R_c-value can be derived from the RF curve of any given wall, using any arbitrary time interval, because the effect of the thickness, even in a short time interval, will always appear in the RFs of much higher index. More explanations about this notion is found in Section 3.5. For short time intervals, the number of wall's needed RFs increases significantly. Therefore the accuracy of R_c-value determination drops, if fewer number of RFs are used in Eq. (2) [57]. This becomes problematic in practice because the experimental error associated with such approach can be higher than the necessary level of accuracy, when (2) is used. Therefore, it is of high importance to confirm the coverage of $2\tau_r|_{1\%}$ in the X RFs, either by observing a rise in Y RFs during the test, measuring the response time before the test, or by monitoring the ratio between two consecutive X RFs (See Section 3.5).

3.4. Response time and RFs' time interval: multi-layered walls

Heterogeneous multi-layered walls are common in buildings. The behaviour of RFs in terms of energy conservation is the same as homogeneous walls: The overall heat applied to one side is stored and conducted to the other side. The magnitude of RFs and their profiles though are versatile. In this section, the behaviour of common two-layered walls is studied. The same principles are valid for walls of more than two layers. The instantaneous heat fluxes at two sides A and C, and at the contact surface B of a two-layered wall of layers (1) and (2), excited by a triangular surface temperature pulse at side A can be calculated based on the temperature history and the theory of RFs as follows [13]:

Combining the second and the third equations with the first and the forth, a global form of equations can be derived:

$$\dot{q_A^t} = \left\{ X_{(1)} - \frac{Y_{(1)}^2}{Z_{(1)} + X_{(2)}} \right\} [T_A^t \cdots T_A^{t-n}] - \left\{ \frac{Y_{(1)} Y_{(2)}}{Z_{(1)} + X_{(2)}} \right\} [T_C^t \cdots T_C^{t-n}] = [U][T_A] - [V][T_C] \tag{12}$$

$$\dot{q_C^t} = \left\{ \frac{Y_{(1)} Y_{(2)}}{Z_{(1)} + X_{(2)}} \right\} [T_A^t \cdots T_A^{t-n}] - \left\{ Z_{(2)} - \frac{Y_{(2)}^2}{Z_{(1)} + X_{(2)}} \right\} [T_C^t \cdots T_C^{t-n}] = [V][T_A] - [W][T_C] \tag{13}$$

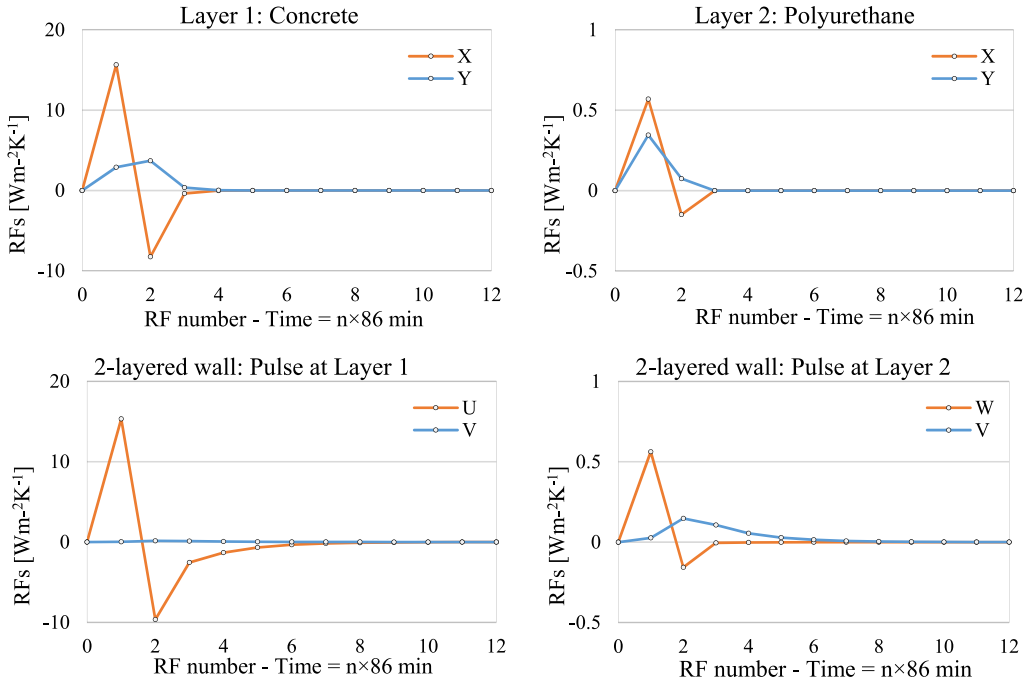

Fig. 9. RFs (dots) from two different layers of the 2-layered wall individually (top) and of the composed wall (bottom). The RFs of the composed wall are a combination of the two layers.

where U, V, and W are the time-series RFs of a two-layered wall. The RFs in brackets are subjected to element-wise operations. In Fig. 9, a COMSOL RF simulation of a two-layered wall with properties introduced in Table 3 is shown.

Note that this construction is shown for demonstration purposes. In practical conditions, the insulation layer is coated with plaster and finishing, whose effect is always included in the RFs of the wall, due to its short response time. The excitation pulse is applied once individually at each slab as a single-layer and then at the two-layered wall: once at side 1 (concrete, left) and once at side 2 (Polyurethane, right). The global $\tau_r|_{1\%}$ and the R_c-value are 43 min and 2.52 $W\,m^{-1}\,K^{-1}$ respectively.

The relationship between$\tau_r|_{1\%}$, t, and RFs as discussed in Section 3.3 can be extended to multi-layered walls. The Pulse and the behaviour of its corresponding response are tied to the thermal response time of different layers. Consider the second surface of the first layer as the first surface of the second layer. The heat pulse will reach the second layer after a period of $(\tau_r|_{1\%})_{(1)}$,the response time of the first layer. Therefore, similar to the outdoor surface for the homogeneous wall, the X curve can be affected by the second layer, only after $2(\tau_r|_{1\%})_{(1)}$ is passed during

Table 3
Construction and properties of the two-layered wall used for simulation of RFs in multi-layered walls.

Layer/property	L [m]	k [W m^{-1} K^{-1}]	ρ [kg m^{-3}]	C [J kg^{-1} K^{-1}]	$\tau_r\|_{1\%}$ [min]	R_c
1: Concrete	0.1	0.7	1600	880	34	0.14
2: Polyurethane	0.05	0.02	35	1320	9	2.38

Table 4
RFs corresponding to different conditions of time interval: The X_0RFs represent both layers, only when the selected time interval is longer than twice the minimum response time of the first layer.

Pulse at Polyurethane Side $(\tau_r\|_{1\%})_1 = 9$ [min]$(\tau_r\|_{1\%})_2 = 34$ [min]X_0 [W m^{-2} K^{-1}]				Pulse at Concrete Side $(\tau_r\|_{1\%})_1 = 34$ [min]$(\tau_r\|_{1\%})_2 = 9$ [min]X_0 [W m^{-2} K^{-1}]			
Condition	t [min]	X_0	$X_{0_{(1)}}$	Condition	t [min]	X_0	$X_{0_{(1)}}$
$t < (\tau_r\|_{1\%})_{(1)}$	2	2.0	2.0	$t < (\tau_r\|_{1\%})_{(1)}$	5	63.5	64.0
	5	2.1	2.1		10	45.0	45.0
	7	1.9	1.9		25	28.2	28.5
$t = 2\tau_{r1}$	18	1	1.1	$t = 2(\tau_r\|_{1\%})_{(1)}$	70	17.1	17.3
$2(\tau_r\|_{1\%})_{(1)} < t < \tau_r\|_{1\%}$	30	0.8	0.9	$2(\tau_r\|_{1\%})_{(1)} < t < \tau_r\|_{1\%}$	NaN	NaN	NaN
$t \approx 2\tau_r\|_{1\%}$	86	0.56	0.6	$t \approx 2\tau_r\|_{1\%}$	86	15.3	15.6
$t > 2\tau_r\|_{1\%}$	200	0.46	0.51	$t > 2\tau_r\|_{1\%}$	200	9.5	11.0
	300	0.44	0.47		300	7.2	9.6
	400	0.43	0.46		400	5.7	8.9
	600	0.42	0.44		600	4.0	8.3
	1000	0.41	0.43		1000	2.6	7.7

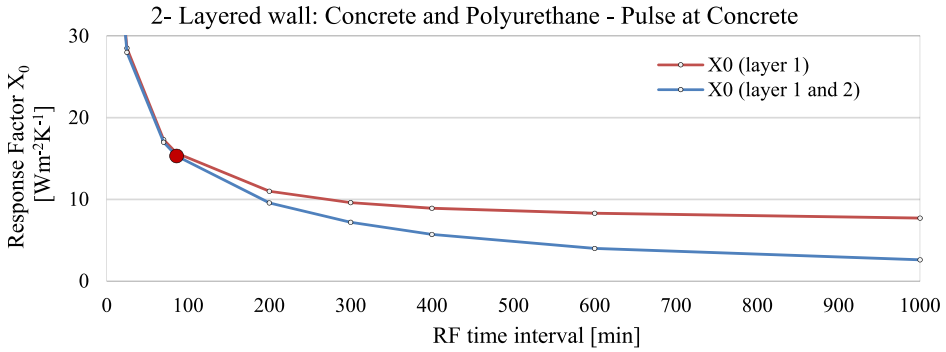

Fig. 10. Relationship between X_0 RF and the RF time interval for a double-layered (concrete and Polyurethane) wall where the excitation pulse is applied to concrete side.

the appearance of X RFs. Accordingly, the X curve of a multi-layered wall is partially/globally influenced by a each layer and its opposite surface, depending on the response time $\tau_r|_{1\%}$ of each layer. Nevertheless, according to energy conservation, the extraction of the R_c-value from the RFs is independent from the aforementioned influence and can theoretically (with infinite number of RFs) take place, unless using a too short time interval where the error in the residuals are known to disturb the accuracy. In Table 4, the results of a simulation are shown in which a two-layered wall (polyurethane and concrete) is excited with pulses of different time intervals. Consider $(\tau_r|_{1\%})_{(1)}$ and $(\tau_r|_{1\%})_{(2)}$ the minimum response times of layers 1 and 2 respectively and $\tau_r|_{1\%}$ the total response time of the wall (the sum of the two response times).

As seen in Table 4 and Fig. 10, the X_0 RFs of the first layer and the whole wall are identical in short time intervals. The RFs are representative for the whole wall (The sum of the RFs is equal to the R_c-value of the whole wall and not the first layer or a part of the wall), when the time interval is longer than twice the total response time. This difference is larger when the pulse is applied at the concrete side, due to the fact that the insulation layer has a much higher influence on the heat transfer phenomenon in comparison with the concrete layer. As shown in Fig. 10, the X_0 values for the whole wall and for the first layer deviate when a time interval longer than twice the response time (red dot) is applied.

The aforementioned argument for X_0 is also valid for RFs with higher index. An X RF with any index is influenced by the second layer/ opposite surface, only when the sum of time intervals (total time duration) before the appearance of that X RF, is longer than twice the minimum response time of the layer (s) ahead/ the whole wall.

Accordingly in Fig. 10, long before the red dot (when a time interval much shorter than $2\tau_r|_{1\%}$ is chosen), it may be that many more of the RFs are not representative for the whole wall, but only representative for the first layer. In this case, if a limited number of RFs are measured and used, the determination of the R_c-value will be associated with inaccuracy. This becomes more problematic when the front layer is non-insulated and the latter layer is an insulation layer, having a much larger influence than the first layer on the total thermal resistance while being excluded from the results. In such case, the inaccuracy level will be much higher than the case where the front layer is an insulation layer.

An accurate R_c-value can be obtained in such cases, only if at some point in the remaining RFs, the effect of the outdoor surface has appeared. This can be confirmed by observation of the rise in Y RFs during the test, measuring the $\tau_r|_{1\%}$ in advance, or by monitoring the ratio between two consecutive X RFs for a sufficiently long period of time (See Section 3.5).

3.5. High-indexed RFs in single-layered and multi-layered walls

In order to spare time in EPM, the X RFs with higher index ($n >> 2$) were not measured, but estimated. The fact that the higher indices form a series in the X graph, and that these RFs are based on the same equation, implies that the RFs with higher index be estimated based on the ones measured. This ratio, also called the common ratio, becomes constant after a certain index [64]. For a homogeneous slab the ratio of the two RFs is:

$$j \gg 2;\ \gamma_i = \exp\left(-\frac{i^2\pi^2\alpha t}{L^2}\right);\ \frac{X_{j+1}}{X_j} = \frac{\sum_{i=1}^{\infty}[(\gamma_i^{j+2} - 2\gamma_i^{j+1} + \gamma_i^{j})/i^2]}{\sum_{i=1}^{\infty}[(\gamma_i^{j+1} - 2\gamma_i^{j} + \gamma_i^{j-1})/i^2]} = D = cte \tag{14}$$

where α is thermal diffusivity, L is the thickness, t is the time interval, and j (the superscripts are powers) is the index of RFs [13]. Accordingly, knowing a limited number of X RFs, the rest can be calculated, provided that the ratio between the known RFs is constant. As this ratio is also found in the literature to have a relationship with properties such as thermal diffusivity, it can be used to determine them in case of

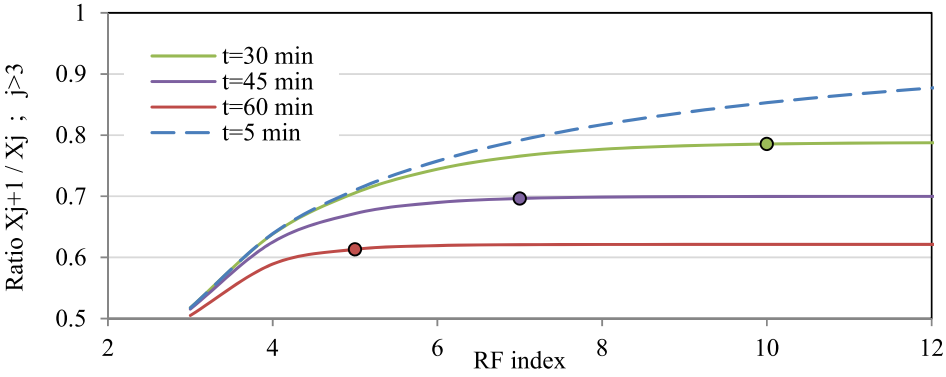

Fig. 11. The ratio between two consecutive RFs: In long time intervals where the R_c-value is calculated successfully, the slope becomes zero as the ratio is constant. The RFs are then representing the whole wall.

interest. As discussed in Section 3.2, for estimation of the R_c-value in a homogeneous wall, the important condition is that the effect of the exterior surface is included in the results. In addition to what was discussed, the effect can be found through the ratio between every two RFs with an index higher than 2. In a homogeneous wall, one can know if the results represent the whole sample, when the ratio $\frac{X_{j+1}}{X_j}$ becomes constant. In Fig. 11, a standard 21 cm brick wall ($k = 0.9\ \mathrm{W^{-1}\ K^{-1}}$, VHC = 136 E5) is shown. The wall is excited with pulses of different time intervals, resulting in different stabilizing points. The RFs of longer time interval reach a constant ratio of D at an earlier index, resulting in an R_c-value representative for the whole wall. For a very short time interval (5 min in dashed blue), the ratio is not yet constant, after 12 RFs. In this case, the R_c-value is smaller, representing only a part of the wall and therefore is inaccurate. In contrast, in the longer time intervals (solid lines), the ratio is constant and the accurate R_c-value has been extracted successfully. It is seen in all graphs that only after twice the response time (4 h) the ratio becomes constant, implying that the effect of the outdoor surface is included in the RFs. Note that in any time interval, the ratio becomes constant at a certain point (RF index m in Eq. (15)). Considering the fact that the RFs reach a constant ratio at index m (large dots in Fig. 11) of their time-series, R_c-value is achieved from the sum of RFs as follows:

$$R_c^{-1} = \sum_{j=0}^{n} X_j = \sum_{j=0}^{m} X_j + \sum_{j=m+1}^{n-1} X_j = \sum_{j=0}^{m} X_j + \sum_{i=0}^{n-1} D^i.\, X_{m+1}$$
$$= \sum_{j=0}^{m} X_j + X_{m+1}(1 - D^n/1 - D) \tag{15}$$

As the sum of the infinite geometric series converges to a limited value, for a large number of RFs, the sum of the RFs converges to the following value:

$$n \to \infty: R_c^{-1} = \sum_{j=0}^{\infty} X_j = \sum_{j=0}^{m} X_j + X_{m+1}(1 - D)^{-1} \tag{16}$$

This implies that in theory, when it is possible to use large number of RFs, the sum of the RFs can be used to calculate the R_c-value, regardless of the time interval used.

Similar to the single-layered walls, the effect of different layers and the exterior surface in a multi-layered wall are conditionally included in the ratio between measured RFs. This phenomenon takes place when the experiment time is longer than at least twice of the total thermal response time. The constant ratio found after 2 $\tau_r|_{1\%}$ (can be found from the rise in Y RFs) can be taken as the one to calculate the remaining RFs. In case the Y RFs are not observed, it is likely that the constant ratio changes to another constant value. This means that the effect of the later layer(s) is included in the X RFs. The effect of each layer is included in the X RFs, just after twice the response time before reaching that layer is passed. In Fig. 12, this is shown by making a comparison between the X ratios in a 2, 3, 4, and a 6 – layered wall. For all four walls, the ratio is constant until the 10th RF. After the 10th, the effect of the fourth, fifth, and the sixth layers can be seen by the sudden change in the slope. This happens due to the fact that twice the total minimum response time of the layers before the 4th layer is covered at the point by which the mentioned RF ($j = 10$) has appeared. The constant ratio moves then towards another constant, showing that the effect of later layers is included in the results. Note that such constructions (6 layers: three layers of brick-insulation) are only for demonstration of RFs and may be non-existent in practice.

The change in the RF ratio slopes in Fig. 12 show how the effect of different layers are included in the X RFs. Monitoring the slopes and observing the changes in the common ratio between X RFs, one can indicate the presence of different layers and therefore indication of the internal composition in a wall of unknown construction.

4. Inverse determination of thermo-physical characteristics using EPM

Reflecting the necessity of reliable estimation of thermo-physical properties, in this section, the RFs are used to calculate the two main thermo-physical properties: thermal conductivity (k) and VHC (ρC). These two parameters are even more important than the R_c-value because the R_c-value can be calculated when k is known (The thickness of a wall can be measured in several ways). The VHC can be used to achieve a more accurate estimation of the thermal behaviour and is needed in dynamic building simulations. Unlike the yearly heating demand, the heating and the cooling capacities and the size of the HVAC installations highly depend on this property [39]. Originally, the X RFs of index 0 to n are calculated for a homogeneous wall, based on the two properties k and VHC, L the thickness, and t the time interval [13]:

$$\begin{cases} X_0 = -\frac{kL}{\alpha t}\left[-\frac{1}{3} - \frac{\alpha t}{L^2} - \frac{2}{\pi^2}\sum_{i=1}^{\infty}\frac{\exp\left(-\frac{i^2\pi^2\alpha t}{L^2}\right)}{i^2}\right] \\ X_1 = -\frac{kL}{\alpha t}\left[\frac{1}{3} + \frac{2}{\pi^2}\sum_{i=1}^{\infty}\frac{\left[\exp\left(-\frac{i^2\pi^2\alpha t}{L^2}\right)\right]^2 - 2\left[\exp\left(-\frac{i^2\pi^2\alpha t}{L^2}\right)\right]}{i^2}\right] \\ X_j = -\frac{2kL}{\alpha t\pi^2}\sum_{i=1}^{\infty}\left(\left[\exp\left(-\frac{i^2\pi^2\alpha t}{L^2}\right)\right]^{j+1} - 2\left[\exp\left(-\frac{i^2\pi^2\alpha t}{L^2}\right)\right]^{j} \right. \\ \qquad \left. + \left[\exp\left(-\frac{i^2\pi^2\alpha t}{L^2}\right)\right]^{j-1}\right)/i^2;\ j \geq 2 \end{cases} \tag{17}$$

where α is thermal diffusivity, On the contrary, in EPM, the RFs can be obtained directly from the measurements and therefore known. Since the wall's thickness is often measurable and the time interval is arbitrarily chosen, the above RF equations can be applied to calculate thermal conductivity and the VHC of the tested sample. With an accurate estimation of thermal conductivity, the thermal resistance can also be calculated, based on the thickness of the wall. As the number of equations is much larger than the number of unknowns, an over-determined system of equations needs to be tackled. Accordingly, the two unknowns, thermal conductivity and the VHC are found, solving the following optimization problem with at least two RFs (equations):

$$\begin{cases} X_0 = f_0(k, \rho C) \\ X_1 = f_1(k, \rho C) \\ X_{j>1} = f_j(k, \rho C) \end{cases} \underset{k,\rho C}{\mathrm{Min}}$$
$$\sqrt[2]{|X_0^* - f_0(k, \rho C)|^2 + |X_1^* - f_1(k, \rho C)|^2 + \sum_{j=2}^{n}|X_j - f_j(k, \rho C)|^2}$$
$$\text{s. t.}\quad k \in [0, 2];\ \rho C \in [2E5, 2E6] \tag{18}$$

The search domains are taken between the minimum and the maximum possible values for building materials. The steps (mesh size) are taken as $1000\ \mathrm{J\,m^{-3}\,K^{-1}}$ for VHC and $0.01\ \mathrm{W\,m^{-1}\,K^{-1}}$ for thermal conductivity. Having an estimation of the materials used in a wall, shorter ranges can be applied. For this method, it is crucial that the RFs represent the desired layer/ wall. Therefore, it is essential to make sure the RFs are of corresponding time intervals. The optimization problem is stated, based on minimizing the RMSE (Root Mean Square Error) of the difference between measured RFs and the RFs calculated based on the wall's properties. The RSME is chosen because it magnifies the tolerances of RFs (e.g. measurement errors) before the square-root and therefore it is more suitable than the MAE (Mean Absolute Error) for the aforementioned problem. However, on the tested samples, MAE has shown similar results. This may change in case of larger operational and equipment errors. In this problem, the objective function has many local minimums. Due to the limitation domain (tolerance), the minimum required steps for the parameters, and the function itself, the computation time is inexpensive. Accordingly, the global minimum is

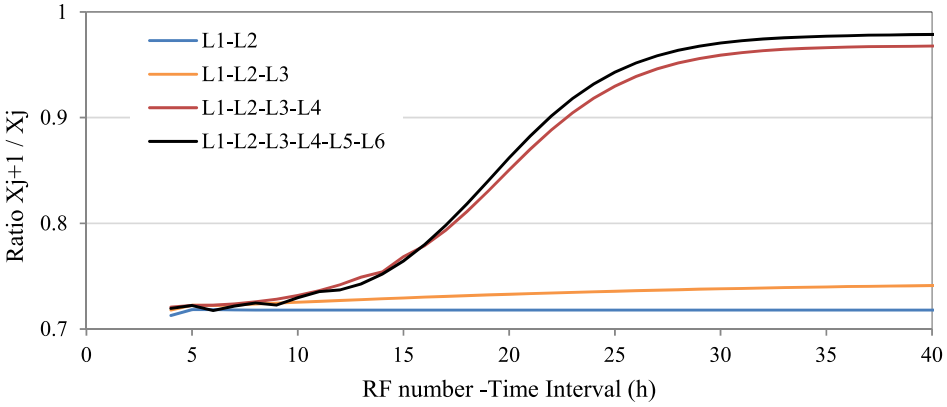

Fig. 12. The change in ratio between two consecutive RFs: X_{n+1}/X_n for $n > 3$ in higher indices in multi-layered walls: The ratio of the two RFs changes in higher indices in a multi-layered wall. The constant ratio moves to another constant value, where the influence of the latter layer(s) is included.

found via Brute-force search [65]. This method solves the problem for all given possibilities to find the minimum of all the given solutions.

4.1. Single-layered homogeneous walls

In homogeneous walls, in addition to the thermal conductivity and VHC, the thickness can also be obtained, solving the following problem for (minimum) three parameters:

$$\begin{cases} X_0 = f_0(k, \rho C, L) \\ X_1 = f_1(k, \rho C, L) \\ X_{j>1} = f_j(k, \rho C, L) \end{cases} \underset{k,\rho C}{\text{Min}}$$

$$\sqrt[2]{|X_0^* - f_0(k, \rho C, L)|^2 + |X_1^* - f_1(k, \rho C, L)|^2 + \sum_{j=2}^{n} |X_j - f_j(k, \rho C, L)|^2}$$

$$\text{s. t.} \quad k \in [0, 2]; \ \rho C \in [2E5, 2E6]; \ L \in [0.1, 0.5] \tag{19}$$

The step size for the thickness is taken as 1 cm. The outcomes of the optimization problem have shown to be more sensitive to X_0 and X_1 rather than to X RFs of higher indices (greater than 2). Regarding the time cost to measure the RFs, this is an advantage when applying large time intervals as it shortens the total measurement period (For k and VHC only 2 RFs can be required). Note that for an additional determination of the thickness, at least 3 RFs are required. In Table 5, the method has been applied to a brick wall with known properties (Theory column), using 5, 3, and only 2 RFs, showing the accuracy of the computation method.

The difference between the estimated values and the actual ones depends on the representativeness of the used RFs. In Table 5, all values, from the extreme case of the 50 cm wall to the 10 cm one, have been determined with 100% accuracy due to the fact that the time intervals is selected as such that all X RFs include information regarding the whole wall. Note that for such high accuracy, for the heavy 50 cm wall, 2 × 1500 min is required to measure the parameters. This time duration (2 days) in comparison to the standard method which requires minimum 3 days of measurements, is still shorter, especially because of high thermal mass in this case which leads to much longer measurement periods if the standard method is to be followed.

Determination of the thermo-physical properties in multi-layered walls requires the use of multi-layered wall equations. For a two-layered wall for instance, U and W in Eqs. (12) and (13) can be used. Note that due to the larger number of unknowns in such cases, more RFs are needed to be measured. As the number of unknowns grows as a result of multi layers, the problem tends towards becoming ill-conditioned.

4.2. Multi-layered walls

In a multi-layered wall, properties of the outer single layers can be determined using EPM, provided that the corresponding RFs contain information only regarding that specific layer. As discussed in previous sections, this can occur in case of a time interval shorter than double the minimum response time of that single layer. An example of the wall introduced in Table 3 is shown below, where the pulse has been applied at the polyurethane once with a time interval of 5 min and once with 18 min (both shorter than the response time of first layer). As shown in Table 6, using RFs of 5 and 18 min time intervals, the optimization can reveal the properties of the first layer.

This fact is used in the next section to calculate the properties of the internal facing layer of a cavity wall.

Table 5
Estimation of thermal conductivity (k), VHC, and thickness (L) using 5, 3, and 2 RFs (equations) for two standard brick walls of 0.2 m and 0.1 m thickness respectively. The effect of adding extra RFs in lighter walls and/or longer time intervals is negligible. (Here, the RFs used for property estimations are obtained by simulation).

Property	Theory	Estimation Using 5 RFs	Estimation Using 3 RFs	Estimation Using 2 RFs	$\tau_r\|_{1\%}$	t
k	0.9	0.9	0.9	0.9	642 [min]	1500 [min]
ρC	1,360,000	1,360,000	1,360,000	1,360,000		
L	0.5	0.5	0.5	N/A		
k	0.9	0.9	0.9	0.9	102 [min]	210 [min]
ρC	1,360,000	1,360,000	1,360,000	1,360,000		
L	0.2	0.2	0.2	N/A		
k	0.9	0.9	0.9	0.9	26 [min]	60 [min]
ρC	1,360,000	1,360,000	1,360,000	1,360,000		
L	0.1	0.1	0.1	N/A		

Table 6
Optimization results: Using RFs of the wall (demonstrated in Table 3) with time intervals shorter than the minimum response time of each layer results in determination of the properties of that single layer.

	Pulse at Polyurethane: $\tau_r\|_{1\%}$ = 9 min		Pulse at Concrete: $\tau_r\|_{1\%}$ = 34 min	
Property	Theory	Estimation Using t = 5 min	Theory	Estimation Using t = 25 min
k	0.02	0.02	0.7	0.7
ρC	46,200	43,000	1,408,000	1,321,000

4.3. Determination of k and ρC from the results of the experiments

The properties of the tested wall can be estimated through the RFs calculated from the results of an EPM experiment. Accordingly, the two main properties have been determined based on the RFs calculated from the experiments, by solving the following optimization problem using only two first RFs.

$$\begin{cases} X_0 = f_0(k, \rho C) \\ X_1 = f_1(k, \rho C) \end{cases} \quad \underset{k,\rho C}{\text{Min}} \sqrt[2]{|X_0^* - f_0(k, \rho C)|^2 + |X_1^* - f_1(k, \rho C)|^2}$$
$$s.\ t. \quad k \in [0, 2];\ \rho C \in [2E5, 2E6] \tag{20}$$

The selected time interval in all experiments has been shorter than $2\tau_r|_{1\%}$ of the first layer, the wood- cement board (146 min). Consequently, as discussed in Section 3.4, the measured RFs include only the properties of only the first layer (wood-cement in Table 1). In Fig. 13, the problem, solved for the theoretical values (k=0.35 W m^{-1} K^{-1} and VHC ρC=1,837,500 J m^{-3} K) is shown, finding the same values for both parameters.

Solving the optimization problem for the results of the experiments leads to a prediction of the thermal conductivity and VHC. The results of the computations are shown in Table 7.

Although closest to the expected value in thermal conductivity, the VHC has shown a large difference when a short time interval is used. This is in-line with the result from another test carried out on a case study whose thermal resistance was measured in [8].

4.4. Accuracy and precision analysis

For an estimation of the accuracy in determination of thermal conductivity and VHC, the results are analysed by making a comparison between the theoretical values of the wall being tested and the ones obtained from the experiments. It is assumed that the actual values are identical to the theoretical values. Note that as the response time of the first layer of the wall (73 min) is longer than any of the time intervals being used, the RFs obtained from EPM consequently refer only to the first layer. The departure is calculated as (21) and the results are summarized in Table 8:

$$Dep\ \ k = 100(k - k^*)/k;$$
$$Dep\ \ \rho C = 100(\rho C - \rho C^*)/\rho C \tag{21}$$

Table 7
Results of the determinations of thermal conductivity (k^*) and VHC (ρC^*) based on two RFs X_0^* and X_1^* with time interval t and pulse magnitude δ.The layer's minimum response time is $(\tau_r|_{1\%})_1$ = 73 min. Theoretical properties of the tested layer are k= 0.35 W m^{-1} K^{-1} and ρC= 1,837,500 J m^{-3} K.

Test	1	2	3	4
t [min]	24	18	26	57
δ [K]	51	65	53	62
X_0^* [W m^{-2} K^{-1}]	18.86	22.12	18.26	14.53
X_1^* [W m^{-2} K^{-1}]	−12.74	−13.31	−12.62	−10.5
k^* [W m^{-1} K^{-1}]	0.25	0.38	0.24	0.28
ρC^* [J K^{-1} m^{-3}]	1,654,000	1,092,000	1,705,000	2,200,000

As seen from Table 7, the thermal conductivity of the first layer has been found with 8.5–31.4% difference with the theoretical value. In comparison with the standard method [10] which declares an uncertainty between 14% and 28% for determination of the R_c-value after many days, the difference is found acceptable. The deviation is expected to be a result of various factors including using only two RFs, the difference between actual and theoretical performance (e.g. moisture content and material aging), instrumental and operational error, and the imperfection of the excitation signals, especially in test 2. The prediction of VHC has shown to be poorest in the shortest time interval (18 min). In the other tests, the departure of VHC prediction has been

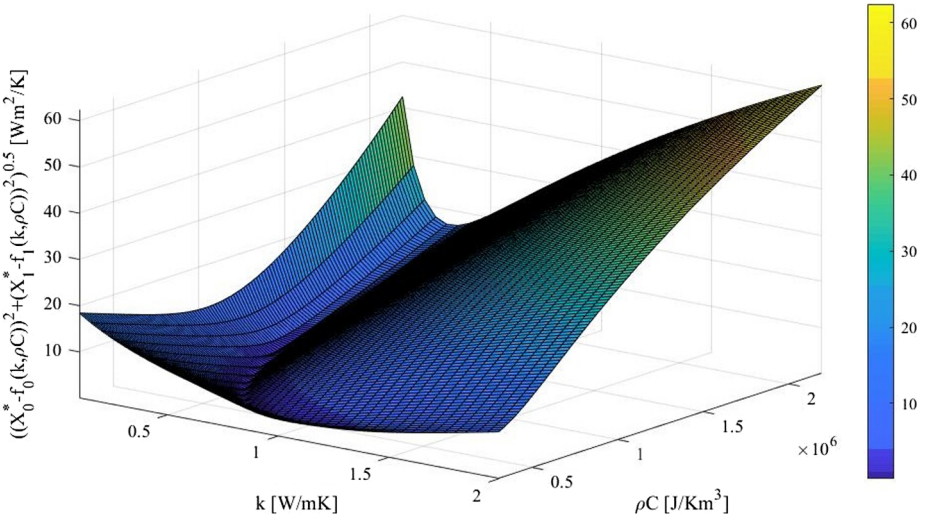

Fig. 13. The surface of RSME ($\sqrt[2]{|X_0^* - f_0(k, \rho C)|^2 + |X_1^* - f_1(k, \rho C)|^2}$) as a function of thermal conductivity (k) and VHC (ρC).

Table 8
The results of departure in estimation of thermal conductivity and VHC from the experiments, using only two RFs. The deviation is the highest for the VHC, when a short time interval is used.

Test	1	2	3	4	Average
Dep k	28.5%	−8.5%	31.4%	20.0%	17.1%
Dep ρC	9.9%	40.5%	7.3%	−19.7%	9.5%

below 20%. The accuracy of the method is expected to be highly improved by improving the control of the signal and therefore minimizing the imperfections seen in Fig. 5.

The instrumental error (based on the accuracy of the equipment) for determination of the thermo-physical characteristics in the experiments at its highest levels occurs at largest values of temperature and heat flux (according to the sensors' manual). Consequently, the final error has been calculated for RFs, using quadrature error computation. Including these errors in the new RFs for the thermal conductivity and VHC determination model (Eq. (18)), by solving the optimization problem with the uncertainty-included inputs, leads to a maximum total error of 11% in determination of thermal conductivity and 42% in the VHC. Note that this is the total error and therefore includes the already-existing error shown in Table 8 (e.g. operation error) of 8.5% and 40.5% for determination of thermal conductivity and VHC, respectively. Accordingly, instrumental error has leaded to a maximum of 1.5% (for VHC) and 2.5% (for k) additional uncertainty. This error is smaller, once a lower heat flux peak (longer time interval) is applied. For determination of the R_c-value, instrumental errors have been illustrated in [8].

Apart from the same range of results in different tests, the precision of the method in general is tested by repeating a test of similar time interval and pulse magnitude. Since the two tests 1 (red dotted) and 3 (blue dashed) are of such condition, they are compared in Fig. 14 where the left graph shows the wall's interior surface temperature pulse (T_s) profiles and the right one shows the X RF curves.

As seen from Fig. 14, the surface temperature profiles and the RFs are in agreement, showing the repeatability and therefore the precision of the method. In addition, the average deviation DEV of the two tests in calculation of thermal conductivity and VHC are calculated (See Table 5):

$$\bar{k} = 0.24 \rightarrow DEV_k = \sum \frac{k-\bar{k}}{2} = \frac{0.2}{2} = 0.01;$$
$$\overline{\rho C} = 1,\ 672,\ 500 \rightarrow DEV_{\rho C} = \sum \frac{\rho C - \overline{\rho C}}{2} = \frac{37,000}{2} = 18,\ 500 \quad (22)$$

The ratios between the deviations and the average values for k and ρC equal 2.6% and 1% respectively, showing the precision of the method. The deviation between the k and ρC values in the four tests are expected to minimize when the control system and the heating and cooling equipment are improved.

5. Conclusion

In the first part of this article, aiming for in-situ determination of the thermal resistance of walls of unknown construction through EPM, a variety of aspects regarding the time interval, the thermal response time, and the excitation pulse magnitude have been illustrated through simulations and experiments. In order to determine the R_c-value accurately, it is always necessary to consider the minimum thermal response time of the wall being studied by its RFs. The X RFs of a wall are representative for its whole construction only when at least double the total response time of the wall is passed. In an EPM experiment on an unknown wall, this can be confirmed in three ways:

1. A rise observed in Y RFs curve is an indication of passing the minimum thermal response time.
2. When the ratio between two consecutive X RFs becomes and stays constant for a long time, double the minimum response time is passed.
3. A test can take place in advance where the time required for the heat flux response at one side to a heat pulse at the other side is measured.

When confirmed, it can be concluded that information related to the composition of different layers and the thickness of a wall is included in its corresponding RFs.

In the second part of this article, it was shown that EPM can be applied to estimate two thermo-physical properties: thermal conductivity and VHC, and to determine the thickness of a homogeneous wall by solving an inverse modelling problem. In addition, in multi-layered walls, the method can be used with homogeneous walls' equations to estimate the aforementioned properties of the outer layers. Accordingly, EPM has been applied experimentally to estimate the thermo-physical properties of a tested case study wall with an acceptable (comparable to the standard method) accuracy and precision. The errors associated with the results are mainly suspected to be a result of poor signal control which was done via a manual dimmer.

Choice of time interval and pulse magnitude

From the simulations and experiments, the possibility and advantage of combining different time intervals and pulse magnitudes has been demonstrated. For the majority of light to medium existing constructions (e.g. 0.1 m–0.3 m brick wall), pulses with time intervals longer than 1 h result in a more stable curve (as a result of easier control and higher robustness) and therefore more reliable outcome. According to the experiments' results, short time intervals also result in poor estimation of VHC. For light-to-medium weighted walls, a time interval of 1 h is found to be sufficient, provided that the considerations regarding the minimum thermal response time are taken into account. Except in

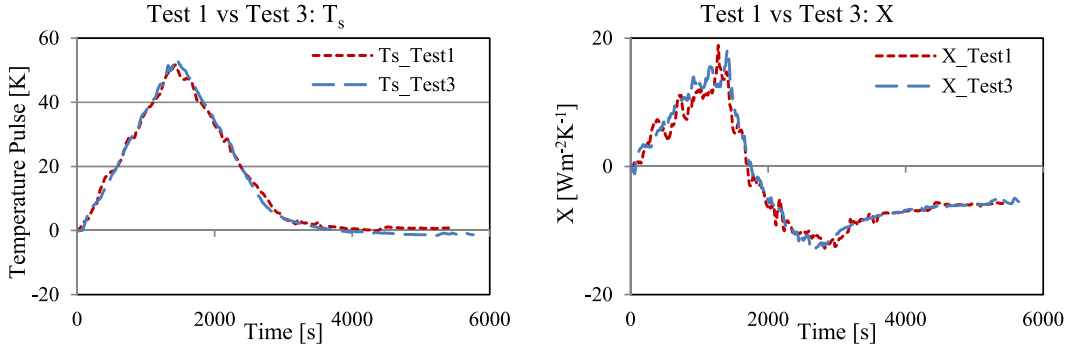

Fig. 14. Surface temperature and RFs measured from two similar tests (1 and 3), showing a good agreement between the trends and the values (a measure of precision of the method), despite the 2 min difference in time intervals.

light walls, the shorter time intervals (30–45 min) result in larger number of smaller RFs and therefore, make the result sensitive to the operational and instrumental errors. Furthermore, using a longer time interval leads to a higher chance of having the effect of latter layers and the opposite surface included in the earlier RFs.

The pulse magnitude may be as large as reaching the surface temperature to 90 °C. Note that the larger pulse magnitudes in small heated areas increase the chances of 3D heat transfer and in that case, using longer time intervals is a more suitable option. Additionally, the location of the insulation in insulated walls can be estimated by comparing the X RFs at two sides. The side with smaller X RFs is closer to the insulation layer.

The ratio between two consecutive X RFs

The ratio between two consecutive X RFs with high index ($j > > 2$) has shown to play an important role in the information that can be extracted regarding the construction of the walls. In a homogeneous wall, the first time this ratio becomes constant, is an indication of the fact that double the minimum response time is passed and the X RFs include information regarding the whole wall. This is an indication of the time when the test can stop and the rest of RFs can be calculated (based on the existing ones) instead of being measured. In multi-layered walls, the change in the constant ratio can give an indication about the presence of different layers. Here too, when the ratio becomes and stays constant, the rest of the X RFs can be calculated instead of being measured.

Determination of characteristics other than the R_c-Value

The results of the simulations have shown the possibility of determination of the thermo-physical characteristics of homogeneous walls by EPM and solving an inverse modelling problem which uses measured RFs and RF equations to estimate thermal conductivity, VHC, and thickness of a homogeneous wall.

In multi-layered walls, the aforementioned properties are expected to be found for each layer, using multi-layered walls' equations. However, this has not been tested so far. Experimentally tested, using only two first RFs and inverse determination, it has been possible to estimate the two thermal properties of the first layer of a cavity wall which has been tested by EPM in less than two hours. Except the short time interval which has resulted in poor estimation of VHC, the other tests have shown reasonably good accuracy and precision for the method.

Limitations in specific typologies

Heavily insulated walls interrupt the 1D heat transfer as they provide a high resistance in the thickness direction. This results in heat transfer in lateral directions. In case of very heavy insulation (this can be detected when no response from the other side of the wall is observed during the experiments), the RFs may represent the properties of the non-insulated layers and only partially the properties of the insulated layer. The part of the insulation being involved in the measured RFs cannot be known in a single test unless the time has passed twice the minimum thermal response time.

The method is not suitable for the cavity walls as the heat pulse cannot be conducted through the air appropriately. The applied heat at one side will dissipate in the air and through combined convection and advection the 1D heat transfer is interrupted. However, only in case of a 3-layered cavity wall, EPM can be applied on two sides separately. This way, relying on the X RFs of each side, the R_c-value of each side as well as their thermo-physical properties can be estimated. Accordingly, the thickness of the two solid layers can be estimated as well. Adding an estimated R_c-value of the air layer to the other two, the R_c-value of such cavity wall can be estimated.

Recommendations for the future studies

The EPM has shown even more potential for its application in future experiments. It is suggested that a more accurate control system is built and used. The size of the heated area as well as the size of the protected surface (at the outdoor side) should be as large as possible. Due to the limitation of the experiments, it is highly recommended to test the method on more constructions. The actual performance of the method on heavy constructions is of interest. Especially in multi-layered walls, the change of the ratio in the X RFs with higher indices can mean a change in the layer in terms of response. It is recommended to study further the ratio and to find more properties, using its constant value. It is recommended to test multi-layered walls to determine the thermal conductivity and VHC of their various layers. Execution of various tests on the same sample is expected to reveal further information about the properties and the construction of the tested sample. The method needs to be further tested in three-layered cavity walls where the pulse is applied at two sides of the cavity. It is recommended to use the method in other components (e.g. floors, roofs, and windows) following required modifications.

Acknowledgements

The Authors would like to appreciate Prof. Staf Roels and Mr. Willem Bertels from the faculty of Civil Engineering in KU Leuven, Leuven, Belgium, for the kind cooperation, arrangements, and providing the test building and the sample.

References

[1] Recast E. Directive 2010/31/EU of the European Parliament and of the Council of 19 May 2010 on the energy performance of buildings (recast). Off J Eur Union 2010;18(06):2010.
[2] Filippidou F, Nieboer N, Visscher H. Energy efficiency measures implemented in the Dutch non-profit housing sector. Energy Build 2016;132:107–16.
[3] Evola G, Marletta L. The Solar Response Factor to calculate the cooling load induced by solar gains. Appl Energy 2015;160:431–41.
[4] Soares N, et al. Laboratory and in-situ non-destructive methods to evaluate the thermal transmittance and behavior of walls, windows, and construction elements with innovative materials: a review. Energy Build 2019;182:88–110.
[5] Liu Y, et al. A novel building energy efficiency evaluation index: Establishment of calculation model and application. Energy Convers Manage 2018;166:522–33.
[6] Majcen D, Itard L, Visscher H. Actual and theoretical gas consumption in Dutch dwellings: what causes the differences? Energy Policy 2013;61:460–71.
[7] Majcen D, Itard L, Visscher H. Theoretical vs. actual energy consumption of labelled dwellings in the Netherlands: discrepancies and policy implications. Energy policy 2013;54:125–36.
[8] Rasooli A, Itard L, Ferreira CI. A response factor-based method for the rapid in-situ determination of wall's thermal resistance in existing buildings. Energy Build 2016;119:51–61.
[9] Ioannou A, Itard L. Energy performance and comfort in residential buildings: Sensitivity for building parameters and occupancy. Energy Build 2015;92:216–33.
[10] ISO, I., 9869: Thermal insulation—Building elements—In-situ measurements of thermal resistance and thermal transmittance. Geneva: International Organization for Standardization; 2014.
[11] ASTM, C., 1046-95 (Reapproved 2001): Standard practice for in-situ measurement of heat flux and temperature on building envelope components. Annual Book of ASTM Standards, vol. 4; 2001.
[12] ASTM, C., 1155-95 (Reapproved 2001): Standard practice for determining thermal resistance of building envelope components from the in-situ data. Annual Book of ASTM Standards, vol. 4, 2001.
[13] Mitalas G, Stephenson DG. Room thermal response factors. ASHRAE Trans 1967;73(1):1–10.
[14] ISO, B., 6946: 2007 Building components and building elements—Thermal resistance and thermal transmittance—calculation method. British Board of Agrément tel.; 1923.
[15] Deconinck A-H, Roels S. Comparison of characterisation methods determining the thermal resistance of building components from onsite measurements. Energy Build 2016;130:309–20.
[16] ISO, B., 8990: 1996, Thermal insulation. Determination of steady-state thermal transmission properties. Calibrated and guarded hot box, BSI, ISBN 0, 1996;580(26826):8.
[17] ASTM. Standard test method for steady-state heat flux measurements and thermal transmission properties by means of the guarded-hot-plate apparatus; 1993.
[18] Asdrubali F, Baldinelli G. Thermal transmittance measurements with the hot box method: calibration, experimental procedures, and uncertainty analyses of three

different approaches. Energy Build 2011;43(7):1618–26.
[19] Ghosh A, Ghosh S, Neogi S. Performance evaluation of a guarded hot box U-value measurement facility under different software based temperature control strategies. Energy Proc. 2014;54:448–54.
[20] Baldinelli G, et al. Dynamic thermal properties of building components: hot box experimental assessment under different solicitations. Energy Build 2018;168:1–8.
[21] Wang F, et al. A data analysis method for detecting wall thermal resistance considering wind velocity in situ. Energy Build 2010;42(10):1647–53.
[22] Cesaratto PG, De Carli M, Marinetti S. Effect of different parameters on the in situ thermal conductance evaluation. Energy Build 2011;43(7):1792–801.
[23] Atsonios IA, et al. A comparative assessment of the standardized methods for the in–situ measurement of the thermal resistance of building walls. Energy Build 2017;154:198–206.
[24] Biddulph P, et al. Inferring the thermal resistance and effective thermal mass of a wall using frequent temperature and heat flux measurements. Energy Build 2014;78:10–6.
[25] Rasooli A, Itard L. In-situ characterization of walls' thermal resistance: an extension to the ISO 9869 standard method. Energy Build 2018;179:374–83.
[26] Tadeu A, et al. In-situ thermal resistance evaluation of walls using an iterative dynamic model. Num Heat Transfer, Part A: Appl 2015;67(1):33–51.
[27] Fokaides PA, Kalogirou SA. Application of infrared thermography for the determination of the overall heat transfer coefficient (U-Value) in building envelopes. Appl Energy 2011;88(12):4358–65.
[28] Aversa P, et al. Infrared thermography for the investigation of dynamic thermal behaviour of opaque building elements: comparison between empty and filled with hemp fibres prototype walls. Energy Build 2017;152:264–72.
[29] Albatici R, Tonelli AM, Chiogna M. A comprehensive experimental approach for the validation of quantitative infrared thermography in the evaluation of building thermal transmittance. Appl Energy 2015;141:218–28.
[30] Lucchi E. Applications of the infrared thermography in the energy audit of buildings: a review. Renew Sustain Energy Rev 2018;82:3077–90.
[31] Buratti C, Moretti E. Thermal resistance of masonry walls: in situ measurements. 6th world conference on experimental heat transfer, fluid mechanics and thermodynamics, Matsushima, Miyagi, Japan. 2005.
[32] Baker P. Technical Paper 2: In situ U-value measurements in traditional buildings–preliminary results; 2008.
[33] Baker P. Technical Paper 10: U-values and traditional buildings-In situ measurements and their comparisons to calculated values; 2011.
[34] Flood C, Scott L, Architects C. In situ thermal transmittance of case studies in Dublin; 2016.
[35] Desogus G, Mura S, Ricciu R. Comparing different approaches to in situ measurement of building components thermal resistance. Energy Build 2011;43(10):2613–20.
[36] Laurenti L, Marcotullio F, de Monte F. Determination of the thermal resistance of walls through a dynamic analysis of in-situ data. Int J Therm Sci 2004;43(3):297–306.
[37] Roulet C, Gass J, Marcus I. In situ U-value measurement: reliable results in shorter time by dynamic interpretation of the measured data. Thermal performance of the exterior envelopes of buildings III. Atlanta (GA, USA): ASHRAE Transactions; 1987. p. 777–84.
[38] Reilly A, Kinnane O. The impact of thermal mass on building energy consumption. Appl Energy 2017;198:108–21.
[39] Corrado V, Paduos S. New equivalent parameters for thermal characterization of opaque building envelope components under dynamic conditions. Appl Energy 2016;163:313–22.
[40] Petojević Z, Gospavić R, Todorović G. Estimation of thermal impulse response of a multi-layer building wall through in-situ experimental measurements in a dynamic regime with applications. Appl Energy 2018;228:468–86.
[41] Evangelisti L, et al. Assessment of equivalent thermal properties of multilayer building walls coupling simulations and experimental measurements. Build Environ 2018;127:77–85.
[42] Šuklje T, et al. An inverse modeling approach for the thermal response modeling of green façades. Appl Energy 2019;235:1447–56.
[43] Alzetto F. Design of experiments for Quick U-building method for building energy performance measurement AU - Ghiaus, Christian. J Build Perform Simul 2019:1–15.
[44] Pandraud G, et al. QUB: a new rapid building energy diagnosis method. Proceedings of CLIMA. 2013.
[45] Boisson P, Bouchié R. ISABELE method: In-situ assessment of the building envelope performances. 9th international conference on system simulation in buildings. 2014.
[46] Sougkakis V, et al. An assessment of the QUB method for predicting the whole building thermal performance under actual operating conditions. International SEEDS conference 2017: sustainable ecological engineering design for society. 2017.
[47] Hiyama K, Kato S, Ishida Y. Thermal simulation: response factor analysis using three-dimensional CFD in the simulation of air conditioning control. Build Simul 2010;3(3):195–203.
[48] Varela F, et al. A direct numerical integration (DNI) method to obtain wall thermal response factors. Energy Build 2014;81:363–70.
[49] Ouyang K, Haghighat F. A procedure for calculating thermal response factors of multi-layer walls—state space method. Build Environ 1991;26(2):173–7.
[50] Sanza Pérez J, et al. A new method for calculating conduction response factors for multilayer constructions based on frequency–Domain spline interpolation (FDSI) and asymptotic analysis. Energy Build 2017;148:280–97.
[51] Chen H, Xiong L, Du C. A simplified dynamic model based on response factor method for thermal performance analysis of capillary radiant floors AU - Yu, Guoqing. Sci Technol Built Environ. 2019:1–21.
[52] Tittelein P, Achard G, Wurtz E. Modelling earth-to-air heat exchanger behaviour with the convolutive response factors method. Appl Energy 2009;86(9):1683–91.
[53] Virseda P, Pinazo J. Thermal behaviour in multilayer products by response factors. J Food Eng 1997;33(3–4):347–58.
[54] Sala JM, et al. Static and dynamic thermal characterisation of a hollow brick wall: tests and numerical analysis. Energy Build 2008;40(8):1513–20.
[55] Martín K, et al. Methodology for the calculation of response factors through experimental tests and validation with simulation. Energy Build 2010;42(4):461–7.
[56] Rasooli A, Itard L, Ferreira CI. Rapid, transient, in-situ determination of wall's thermal transmittance. REHVA European HVAC J 2016;53:16–20.
[57] Rasooli A, Itard L. Properties of the triangular excitation pulse and the 3D heat transfer effects in the excitation pulse method. REHVA 13th HVAC world congress: CLIMA 2019, Bucharest, Romania. 2019.
[58] COMSOL Multiphysics® v. 5.3.a. www.comsol.com. COMSOL AB, S., Sweden.
[59] Hukseflux Thermal Sensors BV, w.h.c., Delft, the Netherlands.
[60] EKO Instruments Europe B.V., w.e.-e.c., Den Haag, Netherlands.
[61] FLIR Systems, I., www.flir.com, Wilsonville, USA.
[62] Deconinck A-H. Reliable thermal resistance estimation of building components from on-site measurements. Belgium: KU Leuven; 2017.
[63] Stewart DB. Time-domain transient thermal response of structural elements. Build Environ 1981;16(2):87–91.
[64] Underwood CP, Yik F. Modelling methods for energy in buildings. Wiley Online Library; 2004.
[65] Trakhtenbrot BA. A survey of russian approaches to Perebor (brute-force searches) algorithms. Ann Hist Comput 1984;6(4):384–400.